Progress in Natural Science: Materials International 26 (2016) 173–176

HOSTED BY

ELSEVIER

Contents lists available at ScienceDirect

Progress in Natural Science: Materials International

journal homepage: www.elsevier.com/locate/pnsmi

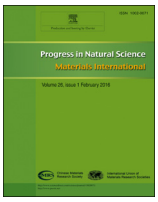

Original Research

Transport dynamics analysis in ferromagnetic heterojunction using Raman spectroscopy and magnetic force microscopy

Ren Ren *, Yijing Ren, Xuan Li, Liya Wen, Song Chen, Ziqiang Wu, Rongdong Xu

Department of Optics Inf., Xi'an Jiao Tong University, Xi'an 710054, China

ARTICLE INFO

Article history:
Received 15 December 2015
Accepted 1 February 2016
Available online 18 April 2016

Keywords:
Metal insulator transition (MIT)
Strong correlated electrons
Positive magnetoresistance
Spin–orbital coupling
Spin–orbit dynamics

ABSTRACT

The $ZnO/La_{0.7}Sr_{0.3}MnO_3$ thin film was epitaxially fabricated on $LaAlO_3$ (100) by pulse laser deposition. The Raman scattering on the single layer LaSrMnO and junction $ZnO/La_{0.7}Sr_{0.3}MnO_3$ was investigated in a giant softening by 490 cm^{-1} John-Teller, 620 and 703 cm^{-1} optical phonon modes. The Raman spectra LaSrMnO and $ZnO/La_{0.7}Sr_{0.3}MnO_3$ were observed with distinct features, i.e., the thickness was in dependent of frequency and intensity. The dynamics results showed that the spin–orbital coupling was caused by anomalies tilt of MnO_6 octahedron. The LSMO/ZnO junction exhibited excellent junction positive magneto-resistance behavior in the temperature range of 77–300 K. The kinetic energy gain was achieved by orbital competition, strong crystal field and charge order of energy band splitting. The transport orbits were in the environment of the ferromagnetic-orbital ordering. The structures of barriers could be adjusted by junction interface and domain boundary condition in terms of the presence of spin–orbital fluctuating.

1. Introduction

The doped manganese oxides $La_{0.7}Sr_{0.3}MnO_3$ (LSMO) shows competition coupling of spins, charge, orbital, and lattice order of freedom, and leads to a mount of phase transition [1–2,4–7]. The single layer $La_{0.7}Sr_{0.3}MnO_3$ is an ideal candidate because of its pronounced two-dimensional structure and magnetoresistance (MR) effect [3]. The orbital transport is coupled to lattice in a low dimensionality. ZnO simultaneously with a wide band gap (3.37 eV) and large exciton binding energy (60 meV) potentially possesses the characteristics of ultraviolet wavelength, high efficiency, lower power, light emitting and laser diodes. This can generate either more promising function or orbital degeneracy. The heterojunction $ZnO/La_{0.7}Sr_{0.3}MnO_3$ nanostructure is a good candidate for fabrication of nanometer-sized optoelectronic devices in ferromagnetic semiconductor [8,9], multilevel resistive switching [10], positive colossal magnetoresistance [11,12], colossal electroresistance [13], manganite tunnel junctions [14], high magnetic sensitivity [15], and ultraviolet fast-response [16]. Moreover, the oxides $ZnO/La_{0.7}Sr_{0.3}MnO_3$ with different carrier transfer and doping lever has recently been carried out.

In this paper, the transfer of $d_{x^2-y^2}$ orbits dynamics coupled to ferro-orbital order state of crystal and carrier transport near the Curie temperature Tc were studied. We measured the SERS (Surface-enhanced Raman scattering spectrum) of LSMO and ZnO thin films. The depletion layer of heterojunction controlled the interface properties. The lattice vibration was observed, and the Raman spectra of crystal lattice vibration modes could reveal ferroelectric transition phase of spin polarization and dielectric properties information. The La/Sr doping ratio, gain size of film and micros-powder, calcined condition, and lattice matching in the LSMO and ZnO thin films heterojunction took effect on phonon frequencies and the direction of lighting. The crystal lattice vibration modes of Raman spectra can reveal the ferroelectric phase transition of spin polarization and dielectric properties information. By changing temperature, film thickness and area, we measured the soft mode frequency to determinate lattice vibration modes, and studied temperature-resistance and the critical size of grain boundary of the heterojunction.

2. Experimental

The crystals of $La_{0.7}Sr_{0.3}MnO_3$ and ZnO were prepared from the analytically pure oxides appropriate stoichiometric proportion by solid state reaction, respectively. The multilayer thin films were annealed at 800 °C with an oxygen pressure 6 Pa for 5 h in order to get better epitaxial character and oxygen doped deposit. The substrate was maintained at 700 °C during the deposition process and then cooled down to room temperature. The LSMO and ZnO layers were successively deposited on the single-crystal LAO (100) substrate by pulse laser deposition. The heterojunction thin film

* Corresponding author.
E-mail address: ren@mail.xjtu.edu.cn (R. Ren).
Peer review under responsibility of Chinese Materials Research Society.

http://dx.doi.org/10.1016/j.pnsc.2016.03.005

was placed in a JanisCCS-300 closed-circuit refrigerator cryostat and the measured temperature ranged from 50 to 350 K. The magnetic field of 0.1, 0.3, and 0.5 T was supplied perpendicularly to the heterostructure. Raman spectra were measured in a quasi-back scattering with the excitation line $\lambda = 514$ nm of Ar laser, 325 nm of solid-state laser, the power of 8 MW. The spectrums were collected by Raman spectrometer (HR800, HORZBA, Jobin Yvon) and a nitrogen cooled charge-coupled device detector. The ZnO film about 75 nm (estimated by profilometer) was masked on $La_{0.7}Sr_{0.3}MnO_3$ (100). The heterojunction had been extensively characterized using XRD, neutron, magnetization, thermal expansion, and magnetoresistivity measurements. The phase structures of the target and orientation of the deposited film were studied by x-ray diffraction.

3. Results and discussions

According to previous researches [17–24] the LSMO has a rhombohedral structure with the R3C space group with O(1) in-plane and O(2) apical oxygen sites as some high-Tc cuprates. The LaO_2 and SrO_2 planes are stacked along a-b axis and separated by the MnO_2 planes as the result of a ferromagnetic-orbital ordering of orbital d_3z^2-r^2 and C-type anti-ferromagnetic (AF) spin ordering below $T = 117$–127 K. Ferroelectric ZnO contains transition metal ions with unpaired *d* electrons. The presence of the *d* electrons can result in a relatively small gap and give rise to a concentration of charged impurities and defects [25]. The question is whether the spin–orbital degrees of freedom are a relevant parameter to describe the properties of $ZnO/La_{0.7}Sr_{0.3}MnO_3$ characteristics.

The LSMO/ZnO heterojunction was characterized by x-ray diffraction pattern, and the results are shown in Figs. 1 and 2. For the LSMO space group R3C, the factor group analysis conformed four Raman-active phonon modes. The Mn^{3+}–O–$Mn^{4+}$and $La(Sr)O_2$ extending modes stretched along the c axis with A_{1g} symmetry. The laser confocal micro Raman spectrometer (HR800 HORZBA, Jobin Yvon), laser light source, were used for the tests with the 325 nm UV laser and optical laser of 514 nm, respectively. The O (2) and La(Sr) vibrations were measured by shifting along the *a* and *b* axis with E_g symmetry.

The spin polarization transport of double exchange mechanics was observed in metal insulate transition, where the substitution

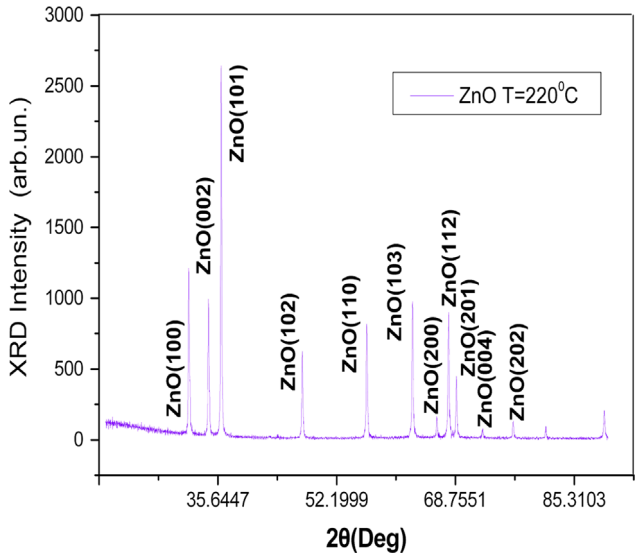

Fig. 1. X-ray diffraction of ZnO.

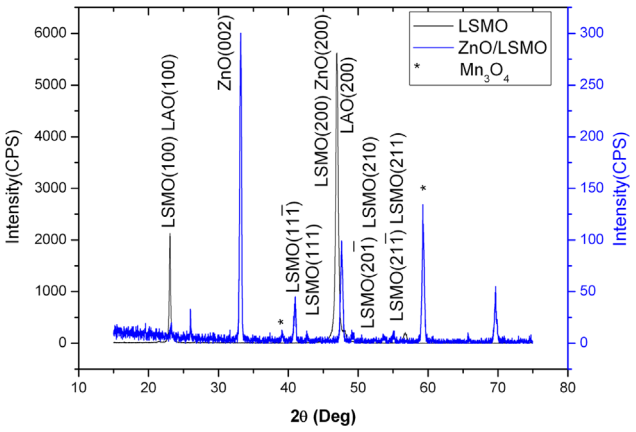

Fig. 2. X-ray diffraction of $ZnO/La_{0.7}Sr_{0.3}MnO_3$/LAO. X-ray diffraction pattern of $ZnO/La_{0.7}Sr_{0.3}MnO_3$/LAO heterostructure. The insets show the (100) and (200) peaks of the LSMO film and LAO substrate.

of divalent alkaline earth element leads to the mixed valence state of Mn:$Mn^{3+}t_{2g}$ 3d and $Mn^{4+}t_{2g}$ 3d. The orbital occupation of diluted $d_{x^2-y^2}$ driven by temperature was in the background of crystal field $d_{3z^2-r^2}$. It is so called spin coupling strongly to the lattice. Moreover, the Mn^{3+}–O^{2-}–Mn^{4+} coupling generates strong ferromagnetic correlation through the charge hopping leading to the anomalous magnetization. The coupled JT effect blurs e_g bands and allows the $Mn^{3+}e_g$ electrons to hop into the empty orbital states [10].

The diffraction peaks of $La_{0.7}Sr_{0.3}MnO_3$/ZnO were matched with the LAO substrate (lattice constant 0.38769 nm) when the lattice constants are 0.386 and 0.379 nm respectively. The LSMO/ZnO structure was characterized by x-ray diffraction pattern shown in Figs. 1 and 2. The inset indicates that the $La_{0.7}Sr_{0.3}MnO_3$ (100) and (200) diffraction peaks occurred at $2\theta = 23°$ and $2\theta = 47°$, while the ZnO (002) (102) (004) diffraction peaks occur at $2\theta = 34°$, $2\theta = 47°$ and $2\theta = 69.7°$, respectively. The results indicate that both the $La_{0.7}Sr_{0.3}MnO_3$ and ZnO thin films both have better epitaxial character. The ZnO film is $2\theta = 34°$ for the (002) orientation with the structure of a hexagonal wurtzite at 220 °C.

Fig. 3 displays AFM results of $ZnO/La_{0.7}Sr_{0.3}MnO_3$/LaAlO. Fig. 4 shows the phonon modes dependence of frequencies and number at 192, 210, 325, 430, 649 cm^{-1}, which rule out impurities and defects as a possible origin. The force microscopy image and further magnetic force microscopy image indicate the interface effect and small effect sizes. The gain size and phase gain boundary take effects to the ferroelectric coupling and mechanical–electrical coupling properties. From LaSrMnO and ZnO of Raman spectra shift, Raman scattering spectrum has four peak at 150, 220, 490, 620 and 703 cm^{-1} in situ growth of LSMO films. The group analysis yields four Raman active phonon modes: Mn–O(2) and (La, Sr)–O(2) stretching modes have shifted along the *c* axis with A_{1g} symmetry, and O(2) and (La,Sr) vibrations displace along the *a* and *b* axes with Eg symmetry. It is shown that LaSrMnO E (TO_1) soft mode is in the first Brillouin zone. LaSrMnO Raman spectrum contains ten kinds of typical single mode E (TO_1), E (LO_1), B_1+E, E

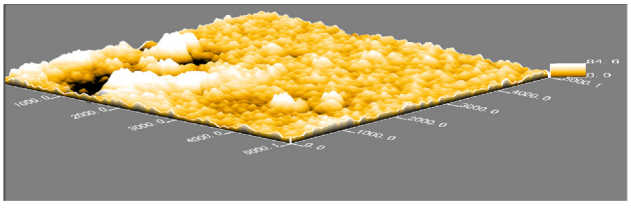

Fig. 3. The atom force microscopy image of surface morphology $ZnO/La_{0.7}Sr_{0.3}MnO_3$/LAO.

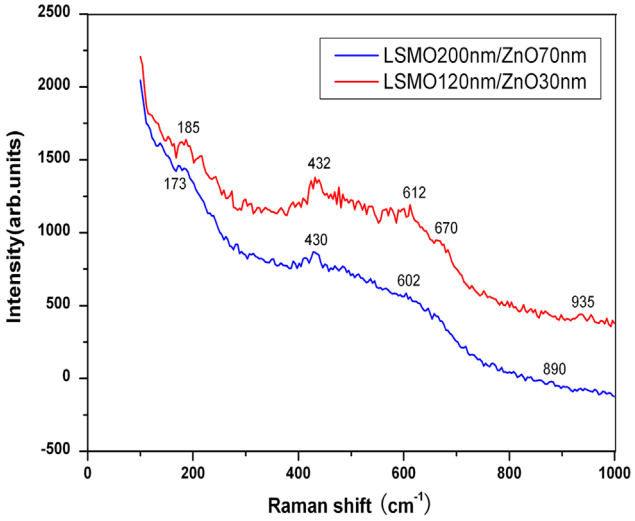

Fig. 4. Raman diffraction spectrum of ZnO/LSMO heterojunction with wavelength of 325 nm laser.

(LO_2), A_1 (TO_2), A_1 (TO_1) E (TO_2), E (two-to-three), $1A_1$ (two-to-three) and A_1 (LO_3). The stretching vibration leads to lattice tilt, rotating of octahedral and vibration of heavy rare metals. If the LSMO has tiny distortion of crystal lattice, the Mn^{3+} and Mn^{4+} atom size correspond to Mn–O chain expansion. These forbidden peaks are weak in intensity but show a well defined symmetry. The Mn^{3+} becomes Mn^{4+} with absorption in oxygen atom, while several Mn^{4+} peaks are observed at room temperature.

It has been observed that the pulse laser deposition made shortage of oxygen in the LSMO thin film. After annealing, the oxygen went into the LSMO lattice, and Mn^{3+} ion becomes to Mn^{4+} ion. Mn^{3+} ion radius (0.07 nm) was more than Mn^{4+} (0.05 nm) ionic radius, which leads to shrinkage 0.04 nm in the lattice constant. With regard to distortion of MnO_6 octahedron, the different spectrum peaks shifted with film thickness. The peak at 490 cm^{-1} moved to low frequency, while the peak at 703 cm^{-1} shifted to high frequency. The two Raman intensity peaks at 703 and 490 cm^{-1} became strong gradually. The Sr^{2+} doping amount on different level not only changed the bond angle and bond length of Mn–O–Mn, but also made the octahedron of MnO_6 distorted. Thus, the Raman peak at 703 cm^{-1} corresponded to the ab in-plane phonon mode. The peak at 490 cm^{-1} connected with ab vertical plane of bended phonon modes. The activated low frequency modes involve (La, Sr)–O(2) or only (Sr, La), and apical O (2) oxygen shifts, because the bonding signal is feeble between the (La, Sr) and O(2) atom [26,27].

The Raman spectrum shows LSMO films diffraction peaks at 310 $cm^{-1}$and 570 cm^{-1} come from different interfaces in thin films. The 490 cm^{-1} is from LAO substrate thin films. The intensity of LAO diffraction peak is weak with the increased thickness. LAO signal hardly appears at the thickness 270 nm. The scattering signals of LSMO 90 nm samples are at 320 cm^{-1}, 480 cm^{-1}, 542 cm^{-1}, 602 cm^{-1}, and 675 cm^{-1}. The characteristic peaks near at 310 cm^{-1} are for the tilt of MnO_6 octahedral. It corresponded to the bond angle changes of Mn^{3+}–O–Mn^{4+}. The scattering peaks at 570 cm^{-1} and 580 cm^{-1} were Jahn Teller transition phase. The peak frequencies of 602 cm, 570, 580 cm^{-1} cm^{-1} correspond to orthogonal cubic phase, which is MnO_6 octahedral stretching of the symmetric and anti-symmetric vibration characteristic peaks. A strong anti-resonance was uncovered at the 190 cm^{-1} mode, which connects to the mixed vibrations of O and La. The octahedral tilt MnO_6 vibration peak is at 310 cm^{-1} which is A_{1g} symmetry. The vibration phonon mode of oxygen atoms is a 'soft mode'. The characteristic peak at frequency 702 cm^{-1} corresponds to the direction of rhombus anti-symmetric stretching mode. A weak A_{1g} phonon signals at the same frequencies of 203 and 310 cm^{-1} were observed in (cc) polarization. The Raman shift corresponded to tilt of MnO_6 octahedral.

The spin polarization determined the phase inverse properties of LaSrMnO and ZnO thin films. The LaSrMnO anti-ferromagnetic order of $d_{x^2-y^2}$ orbits competed with the ferromagnetic order of $d_{3z^2-r^2}$ orbit. The wurtzite ZnO is (P63mc) group structure. Each of the original cells has four atoms. ZnO Raman spectrum has an activated mechanism, such as molecular vibrations, elementary excitation and defects, etc. The first-order Raman spectra involved lattice vibration modes near Bloch area $q=0$, the multi-phonons included $1A_1$, $2B_1$, $1E_1$, and $2E_2$. The spin–orbital couple should be understood by the crystal field effects [28].

Fig. 4 shows Raman diffraction spectrum of ZnO/LSMO heterojunction with laser wavelength 325 nm. In those optical multi-phonon modes, A_1 and E_1 both have Raman and infrared activity. Pure ZnO Raman scattering spectrum at room temperature is identified with five Raman peaks: 379 cm^{-1} corresponds to E(LO) mode scattering peak, 408 cm^{-1} is to the E(TO) scattering peak, 332 cm^{-1} is the process of multi-phonon scattering peak, 583 cm^{-1} corresponds to A1(TO) scattering peak, 437 cm connects to E(H) mode scattering peak, etc, respectively. The Raman peak E_2(H) mode reflects the ZnO wurtzite' features. The other peaks show the ZnO multi-phonons vibration characteristics. A_1(TO) ZnO wurtzite corresponded to defects of ZnO.

Fig. 5 displays temperature dependent of the LSMO/ZnO junction resistance under applied different magnetic field. The insets are temperature dependence of MR at $H=0.1$, 0.3 and 0.5 T. The magnetoresistance is $MR=\Delta R/R=(R_H-R_O)/R_O$, where R_H is the resistance of heterojunction with the magnetic field and R_O is the resistance without the magnetic field. The attracted phenomenon was that the MR behaviors in the LSMO/ZnO heterojunction existed at low temperature and large magnetic field, and represented a positive MR property at the temperature range from 77 to 300 K at magnetic field 0.5 T. The junction resistance and magnetic resistance of LSMO/ZnO for the 2 mV positive bias changed with temperature as depicted in Fig. 5, where the LSMO main phase of heterojunction transfers from the metal to PM insulator occurred at 0.5 T. The junction resistance reduced with the increasing temperature at 0.1, 0.3, and 0.5 T, respectively. In the structure the LSMO/ZnO heterojunction MR had a positive behavior at the temperature range from 50 to 300 K with the magnetic field of 0.1 and 0.2 T.

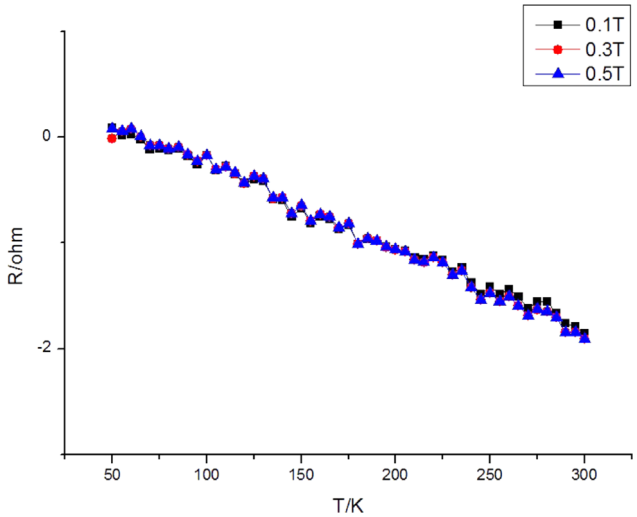

Fig. 5. Temperature dependence of the LSMO/ZnO junction resistance of the heterostructure under applied different magnetic field. The insets are temperature dependence of MR at $H=0.1$, 0.3 and 0.5 T.

Additionally, the multi-phonon scattering was dominated by a resonance induced by an orbital excitation of $d_{3x^2-r^2}/d_{3y^2-r^2}$ orbital order state. As going though the anti/ferromagnetic insulator boundary, the $d_{3x^2-r^2}/d_{3y^2-r^2}$ orbits were rearranged by the lattice alternating. Moreover, the orbits excitons were responsible for the three characteristic peaks of anti-ferromagnetic phase. Finally, they were damped out in the ferromagnetic insulating phase. The multi-phonon scattering was decided by the orbital-ordering model. As a result, the Raman spectral weight of orbital excitons in the ferromagnetic insulating phase shifted to the lower energy compared to the anti-ferromagnetic insulating phase. The double exchange energy of LSMO and localization of holes provided gain, while the ferromagnetic insulating phase balanced energy gain between double exchange energy of LSMO and localization of holes.

4. Conclusions

The carrier orbital transport dynamics property is studied by lattice distortion heterojunction on ZnO/$La_{0.7}Sr_{0.3}MnO_{3-\sigma}$. The junction magnetoresistance properties could be adjusted by orbit-spin, magnetic and lattice field. The surface-enhanced Raman scattering spectrum of doped manganite heterojunction LSMO/ZnO reveals a significant holes mobility and orbital fluctuating. The junction positive magnetoresistance is due to interface field effect and alteration energy band, which are deformed by magnetic structure, crystallographic structure, and carrier concentration. Raman scattering spectrum on the single and multilayer junction LSMO indicates the orbit-spin and lattice coupling. The orbital dynamics shows that orbital coupling is the origin of anomalism lattice. The junction resistance effects with a maximum 33.33% at 0.5 T are observed in the ZnO/$La_{0.7}Sr_{0.3}MnO_3$/LaAlO heterostructure. The study is attributed to the further understanding of charge order, spin–orbital coupling, magnetic order, lattice structure, and development of positive CMR device.

Acknowledgements

This work is supported by National Natural Science Foundation of China (Grant nos. 10775111, 61574115, 51572222, and 61471301).

References

[1] K. Lord, D. Hunter, T.M. Williams, A.K. Pradhan, Appl. Phys. Lett. 89 (2006) 052116.
[2] R. Vonhelmolt, J. Wecker, B. Holzapfel, L. Schultz, K. Samwer, Phys. Rev. Lett. 71 (1993) 2331.
[3] R. Lengsdorf, M. Ait-Tahar, S.S. Saxena, M. Ellerby, D.I. Khomskii, H. Micklitz, T. Lorenz, M.M. Abd-Elmeguid, Pressure-induced insulating state in (La,Sr)CoO_3, Phys. Rev. B 69 (14) (2004) 140403.
[4] R. Vonhelmolt, J. Wecker, K. Samwer, L. Haupt, K. Barner, J. Appl. Phys. 76 (1994) 6925.
[5] A. Rastogi., Phys. Rev. B 86 (2012) 075127.
[6] P. Kumar, R. Mahendiran, Appl. Phys. Lett. 106 (14) (2015) 142401.
[7] J. Wang, J.B. Neaton, H. Zheng, V. Nagarajan, S.B. Ogale, B. Liu, D. Viehland, V. Vaithyanathan, D.G. Schlom, U.V. Waghmare, N.A. Spaldin, K.M. Rabe, M. Wuttig, R. Ramesh, Science 299 (2003) 1719.
[8] Y.C. Wang, R. Ren, C.L. Chen, D.A. Ren, K.X. Jin, X. Yuan, S.G. Zhao, Z.M. Song, Can. J. Phys. 83 (2005) 699.
[9] K. Yamamoto, T. Kimura, T. Ishikawa, T. Katsufuji, Y. Tokura, Phys. Rev. B 61 (2000) 14706.
[10] H. Tanaka, J. Zhang, T. Kawai, Phys. Rev. Lett. 88 (2002) 027204.
[11] X.P. Zhang, B.T. Xie, Y.S. Xiao, B. Yang, P.L. Lang, Y.G. Zhao, Appl. Phys. Lett. 87 (2005) 072506.
[12] H. Katsu, H. Tanaka, T. Kawai, Appl. Phys. Lett. 76 (2000) 3245.
[13] J.X. Zhang, Y.L. Li, S. Choudhury, L.Q. Chen, Y.H. Chu, F. Zavaliche, M.P. Cruz, R. Ramesh, Q.X. Jia, J. Appl. Phys. 103 (2008) 094111.
[14] L.F. Fan, C.L. Chen, B.C. Luo, J. Appl. Phys. 109 (2011) 073716.
[15] A. Tiwari, C. Jin, D. Kumar, J. Narayan, Appl. Phys. Lett. 83 (2003) 1773.
[16] A. Brinkman, Nat. Mater. 6 (2007) 493–496.
[17] P. Moetakef, Phys. Rev. X 2 (2012) 021014.
[18] E. Dagotto, T. Hotta, A. Moreo, Phys. Rep. 344 (2001) 1.
[19] A.E. Sovestnov, A.V. Tyunis, E.V. Fomin, Tech. Phys. Lett. 35 (1) (2009) 26.
[20] S.I. Park, J.H. Son, S.S. Cho, IEEE Trans. Magn. 36 (5) (2000) 2933.
[21] S.Y. Dai, Z.H. Chen, Y.L. Zhou, B.L. Cheng, K.J. Jin, L.F. Liu, G.Z. Yang, X.L. Ma, Appl. Phys. Lett. 86 (2005) 032502.
[22] M. Daghofer, A. Oles, D. Neuber, W. vonder Linden, Phys. Rev. B 73 (2006) 104451.
[23] M. Daghofer, D.R. Neuber, A.M. Oles, W. v d Linden, Phys. Status Solidi B 243 (2006) 277.
[24] K.J. Jin, Q.L. Zhou, K. Zhao, B.L. Cheng, Z.H. Chen, Y.L. Zhou, G.Z. Yang, Phys. Rev. B 71 (2005) 184428.
[25] C. Mitra, P. Raychaudhuri, K. Dörr, K.H. Muller, L. Schultz, P.M. Oppeneer, S. Wirth, Phys. Rev. Lett. 90 (2003) 017202.
[26] K.J. Jin, Y.H. Huang, M. He, K. Zhao, B.L. Cheng, Z.H. Chen, Y.L. Zhou, S.Y. Dai, G. Z. Yang, Appl. Phys. Lett. 86 (2005) 241915.
[27] G. Kim, S.S. Lee, S.C. Wi, J.S. Kang, S.W. Han, J.Y. Kim, B.W. Lee, H.J. Shin, B. G. Parr, J.H. Park, B.I. Min, J. Appl. Phys. 99 (2006) 08Q309.
[28] K. Michaeli, A.C. Potter, P.A. Lee, Phys. Rev. Lett. 108 (2012) 117003.